Microwave Electrothermal Thruster Performance in Helium Gas

S. Whitehair* and J. Asmussen†
Michigan State University, East Lansing, Michigan
and
S. Nakanishi‡
Analex Corporation, Cleveland, Ohio

The description and experimental performance of a microwave electrothermal thruster are presented. This thruster makes use of an internally tuned, single-mode cylindrical cavity applicator to focus and match microwave energy into an electrodeless, high-pressure, flowing gas discharge located inside a quartz discharge chamber. The cavity TM_{011} or TM_{012} modes produced a discharge adjacent to the quartz nozzle and the combination of single-mode focus control and variable, internal cavity matching allowed the continuous experimental operation and measurement over discharge pressures of 40–1100 Torr and flow rates of 8×10^{6} to 150×10^{-6} kg/s. Experimental measurements of microwave coupling efficiency, thruster energy efficiency, and specific impulse are presented for nitrogen and helium discharges. Measured microwave coupling efficiencies to the discharge are in excess of 95%; i.e., the transfer of microwave energy to the discharge is a very efficient process. Experiments which measured hot and cold thruster pressures in helium gas with 200–1200 W of 2.45-GHz input power yielded calculated energy efficiencies of 10–50% and a specific impulse of 200–600 s. Nozzle melting and erosion limited the input power and specific impulse. The measured performance compares favorably with other electrothermal thruster measurements and suggests that design improvements that employ higher-temperature nozzle materials and more efficient discharge chambers could yield a much improved performance.

Nomenclature

A^* = minimum nozzle throat area
C_c = capacitance of excited mode near resonance
C_f = thrust coefficient
C_p = propellant specific heat
$(\text{Eff})_1$ = overall microwave coupling efficiency
$(\text{Eff})_2$ = applicator microwave coupling efficiency
E_r = radial electrical field
E_{r0} = empty cavity radial electric field
F = thrust force
F_c = cold propellant thrust force
F_H = hot propellant thrust force
g = gravitational acceleration
G_c = conductance of excited mode near resonance
GHz = gigahertz (i.e., 10^9 Hz)
G_L = conductance of discharge
I_0 = total input current on the coupling probe
I_{sp} = specific impulse
I_{spc} = cold specific impulse
I_{spH} = hot specific impulse
$j^B L$ = susceptance of discharge
jX = reactance of modes away from resonance
jX_{in} = cavity input reactance
L_c = inductance of excited mode near resonance
$\dot{m}$ = mass flow rate
$\dot{m}_H$ = mass flow rate of hot propellant
$\dot{m}_c$ = mass flow rate of cold propellant
M = molecular weight
p = nozzle inlet pressure
p_c = cold chamber pressure
p_H = hot chamber pressure
P/F = power-to-thrust ratio
P_a = power absorbed in the discharge
P_b = power absorbed in cavity walls
P_i = incident power
P_r = reflected power
P_t = total power absorbed in the microwave cavity
P_{t0} = empty cavity absorbed power
Q = cavity Q
Q_u = loaded cavity Q
Q_{u0} = empty cavity Q
R = intrinsic resistance of the cavity walls
R_{in} = cavity input resistance
S = interior cavity wall surface
TM = transverse magnetic mode
T_0 = gas temperature prior to expansion
T_{01} = discharge inlet temperature
T_{02} = discharge outlet temperature
v_c = exhaust velocity of cold propellant
v_H = exhaust velocity of hot propellant
V = cavity volume
V_L = plasma volume
W_e = time-averaged energy stored in the electric field
W_m = time-averaged energy stored in the magnetic field
Z_{in} = cavity input impedance
η = energy efficiency
ω_p = plasma frequency
ν_{eff} = effective collision frequency for electrons

Received Sept. 27, 1985; revision received April 1, 1986.

*Graduate Assistant, Department of Electrical Engineering.
†Professor, Department of Electrical Engineering. Member AIAA.
‡Mechanical Engineer.

Introduction

RECENT experiments[1,2] with microwave discharges formed at high pressure inside coaxial and cylindrical cavity microwave applicators have demonstrated a new electrothermal thruster concept. In particular, experiments employing microwave discharges in nitrogen gas with 200–2000 W of 2.45-GHz input power have yielded[1,2] energy efficiencies of 10–60% with a specific impulse of 200–280 s. This performance compares favorably with that of other

electrothermal thrusters operating in nitrogen gas,[1,2] and has demonstrated the feasibility of using high-pressure microwave discharges as part of an electrothermal thruster concept. This microwave engine has a number of characteristics similar to those of other electrothermal propulsion concepts such as the resistojet[3,4] and the arcjet.[5] That is, when operating with a low molecular weight gas and at high temperature, it is expected to achieve a higher specific impulse than chemical rockets and with thrust levels much greater than can be obtained from the best of present-day electrostatic ion thrusters.

The principal elements of a microwave electrothermal thruster system are shown in Fig. 1. The system receives its electrical energy from a source such as solar cells and converts it into microwave power via a power conditioner such as a magnetron or klystron. Once converted into "microwaves," the electric energy is coupled into an energy absorption chamber where a low molecular weight gaseous propellant is heated as it flows through the chamber. The heated propellant then exits via a conventional nozzle, producing thrust. Also shown in Fig. 1, but not elaborated upon here, is the potential for the use of beamed microwave or millimeter wave electricity to supply energy to the thruster.[6]

This paper presents experimental measurements which further support the potential of the microwave electrothermal concept. In particular, experimental measurements of the microwave coupling efficiency to high-pressure N_2 and He gas discharges are presented. New experimental performance measurements in He gas excited with the TM_{011} cavity mode are also presented and are compared with earlier measurements[2] made on N_2 gas excited in the TM_{012} mode. These experiments demonstrate that this concept is not limited to a single gas or one electromagnetic mode and show further that the concept is very versatile and can be adapted to many different operating conditions.

Microwave Discharge at High Pressures

The problems of discharge formation, maintenance, and control at high and low pressures in a cylindrical cavity applicator have been discussed earlier.[7-10] At high pressures (>100 Torr), important for electrothermal thruster applications, microwave discharges contract and separate from the surrounding enclosure walls and take on shapes that are related to the field patterns of the exciting electromagnetic modes. That is, microwave arc discharge shapes and positions vary with cavity mode excitation. The formation of contracted and floating microwave discharges has been observed in many experiments.[1,2,8-13]

The physics of discharge constriction and separation from enclosing discharge chamber walls at high pressures has been extensively studied in lower-frequency and DC arcs.[14-17] Although contracted microwave discharges have not been as thoroughly studied, there is reason to believe that the physics of these discharges is similar to the better understood lower-frequency and DC discharges. The few investigations reported[10-13] support this view.

Several features of microwave arc discharges are briefly discussed here to provide a better understanding of the microwave electrothermal concept. The microwave arc, like lower-frequency arcs, is a thermally inhomogeneous discharge. It has a hot central core, and sharp thermal gradients exist between the discharge center and surrounding walls. Microwave energy is readily coupled into the electron gas in the hot discharge center because of its reduced gas density, and neutral gas species are also readily ionized and excited in the hot discharge region.

Major energy losses from the discharge occur by heat conduction, convection, and radiation.[15,16] The large temperature gradient causes heat conduction losses to become an important loss process. This loss mechanism includes the contribution to the heat conductivity by molecules, atoms, electrons, and ions, and also chemical reactions such as the

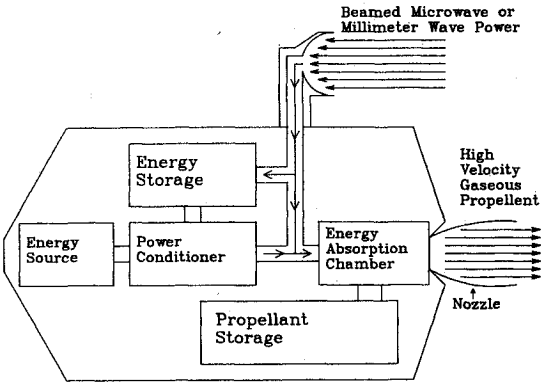

Fig. 1 Block diagram of a microwave electrothermal thruster system.

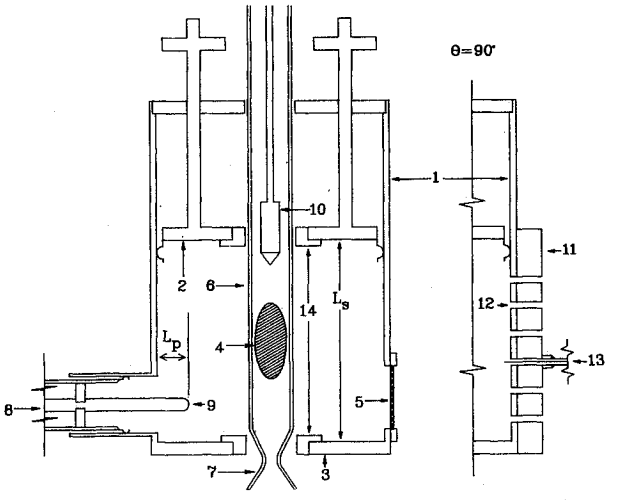

Fig. 2 Cross sectional views of the cylindrical cavity electrothermal thruster. The full cross section is the $\theta = 0$ plane passing through the input probe. The partial cross section $\theta = 90$ deg displays the microcoax inputs. Here L_s is the short position and L_p is the probe position.

transport of dissociation energy and ionization energy to the arc fringes by free radicals and ions.[15] Owing to the high-pressure environment electron, ion and free radicals recombine quickly outside the hot central core and thus convert their dissociation, ionization, and excitation energy into thermal energy. The result is a discharge with radially varying gas temperature, ionization rate, and volume recombination rate. Gas temperature, ionization, dissociation, etc., are highest in the center of the discharge, while volume recombination and de-excitation of the different species increase radially away from the discharge center as the cooler, denser gas regions near the walls are approached. The central discharge core gas temperatures vary with gas type and pressure but typically are in excess of 2000 K, while temperatures external to the discharge are controlled by wall temperatures and the gas temperatures of the gas flowing around the discharge.

Description of Microwave Energy Absorption Chambers

The energy absorption chamber shown in Fig. 1 is made up of two interdependent parts: 1) an energy coupler and 2) a discharge chamber. Initial microwave thruster experiments[1,2] employed two basic energy coupler concepts, called microwave applicators in this paper, in keeping with the present nomenclature for microwave technology. These two concepts were described in detail earlier[1,2] and were classified as coaxial and cylindrical cavity applicators. Each applicator

surrounds and couples microwave energy into a cylindrical discharge chamber consisting of a quartz tube and nozzle. The microwave discharge is maintained in a stable fashion contracted away from the walls of the absorption chamber. All experimental measurements reported in this paper employ the cylindrical cavity applicator shown in Fig. 2.

The cylindrical cavity utilizes the same design philosophy of earlier experiments.[7-9] The resonant portion (or "cavity") is formed by the 17.8-cm-inside-diameter cylindrical brass pipe (1) and the transverse brass shorting planes — or shorts — (2) and (3). One of the shorts (2) is adjustable to provide a variable cavity length of 6–16 cm. The discharge (4), which could be viewed through a copper-screened window (5), is formed inside a cylindrical quartz discharge chamber (6), passing coaxially through the cavity. Input gases are injected at one end of the quartz tube and exit via a nozzle (7) after passing through the discharge zone (4). Input microwave power is fed into the coaxial input port (8) and coupled into the cavity via the adjustable probe (9). A rectangular brass piece (11) was soldered onto the outside of the cylindrical tube (1) parallel to the axis of the cavity. Several small diagnostic holes (12) were drilled through this piece at known axial locations in the cavity wall and small electrical E-field probes (13) made from 2-mm-outside-diameter microcoax were inserted into the diagnostic holes. When calibrated, these probes measured the applicator radial E-field strength near the cylindrical wall with little detectable perturbation to the plasma or cavity fields.

In earlier experiments[2] with N_2 gas a microwave discharge (4) was created in the center of the discharge chamber (6) by exciting the cavity in the single, TM_{012} cylindrical cavity mode. The electric and magnetic field patterns and the associated discharge for this mode are shown in Fig. 3. The electric field has an axial standing wave maximum along the axis producing an intense, approximately half-wavelength discharge in the center of the cavity and the center of the discharge chamber. As shown in Fig. 3, the discharge is "contracted" or separated from the discharge chamber walls. In keeping with lower-frequency arc discharge classifications,[15] this microwave arc configuration can be classified as a wall-stabilized arc. This classification, introduced in connection with arc lamps,[16] is used to describe the discharge stability of arcs enclosed in cylindrical tubes. Such arcs assume a rotationally symmetric, coaxial position inside the tube. Any movement of the arc column toward the wall is compensated by increased heat conduction to the wall, reducing the temperature and the electrical conductivity at this location. Thus this portion of the arc is cooled and the arc is forced to return to its equilibrium position in the center of the discharge. The increased thermal conduction to the walls represents the stabilizing mechanism. It is important to note that if the arc is forced next to the walls by buoyant forces or gas flows or by the exciting electric field geometries, then excessive wall heating and erosion occur.

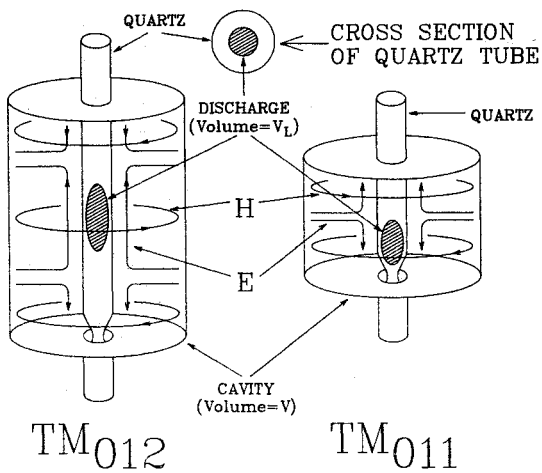

Fig. 3 Electric (E) and magnetic (H) field patterns for the TM_{011} and TM_{012} modes. The discharge cross sections display typical discharge shapes at high pressure (>100 Torr).

Experiments with He gas reported here use the TM_{011} cavity mode, which is also shown in Fig. 3. The electric and magnetic field patterns are similar to the fields of the TM_{012} mode, except the cavity is adjusted to one-half the resonant length, i.e., ~7.6 cm. The discharge is formed at one end of the cavity adjacent to the nozzle and its length is approximately a quarter wavelength long. The advantages of this configuration are that the discharge can easily be brought close to the nozzle and the discharge has a shorter cylindrical length and hence smaller radial surface, which minimizes radial energy losses.

Discharge Coupling, Matching, and Control with Single-Mode Cavity Applicators

An important feature of the cylindrical cavity applicator is its ability to focus and match (little or no reflected power) the incident microwave energy into the discharge zone. This is accomplished with single-mode excitation and "internal cavity" matching. Single-mode excitation allows the focusing and control of the microwave energy into the discharge zone. The matching is labeled "internal cavity," since all tuning adjustments take place inside the cavity.

This method of electromagnetic energy focusing and matching is similar to that employed in recently developed microwave ion sources.[18-20] The differences with this application are associated with different excited cavity modes and the discharge itself, i.e., differences in discharge shape and location and the discharge properties due to the higher operating pressures.

The input impedance of the microwave cavity is given by

$$Z_{\text{in}} = \frac{P_t + 2j\omega(W_m - W_e)}{\frac{1}{2}|I_0|^2} = R_{\text{in}} + jX_{\text{in}}$$

where P_t is the total input power coupled into the cavity (which includes metal wall losses, as well as the power delivered to the discharge); W_m and W_e are, respectively, the time-averaged magnetic and electric energy stored in the cavity fields; $|I_0|$ is the total input current on the coupling probe; and R_{in} and jX_{in} are the cavity input resistance and reactance and represent the complex load impedance as seen by the feed transmission line.

At least two independent adjustments are required to match this load to a transmission line. One adjustment must cancel the load reactance while the other must adjust the load resistance to the characteristic impedance of the feed transmission system. In the cavity applicator the continuously variable probe (9) and cavity endplate (2) tuning provide these two required variations and, together with single-mode excitation, are able to cancel the discharge reactance and adjust the discharge resistance to equal the characteristic impedance of the feed transmission line.

This internal cavity-matching technique can best be understood with the aid of the equivalent circuit shown in Fig. 4. Figure 4 displays a standard circuit representation for a cavity which is connected to a feed waveguide or transmission line and is excited in the vicinity of a single-mode resonance.[21] The variables G_c, L_c, and C_c represent the conductance, inductance, and capacitance, respectively, of the excited mode near resonance, and jX represents the reactive effect of the evanescent modes far from resonance. The relationships between the cavity fields and these equivalent lumped circuit elements are shown in Fig. 4. In a cavity without a discharge, $\epsilon' = \epsilon_0$, $\epsilon'' = 0$, and $V_L = 0$, and integrations for C_c and L_c are over the entire cavity volume V. At resonance, the capacitive and inductive susceptance cancel, resulting in a pure conductive in-

put admittance. The coupling probe (or aperture) is represented as the ideal transformer of turns ratio m:1. Both circuit elements and the transformer are drawn with arrows to indicate their variability during the tuning process.

The discharge is ignited by first adjusting the probe and cavity length positions to excite a specific empty cavity resonance (i.e., TM_{012} or TM_{011}) and to match the empty cavity applicator to the input transmission system. Microwave power is then applied, absorbed into the cavity without reflection, and a discharge is ignited even with low input powers of 20–50 W if the pressure in the discharge zone is reduced to 0.5–10 Torr. The presence in the discharge then changes L_c, G_c, and C_c and adds an additional discharge conductance G_L and susceptance jB_L to the circuit; that is, in the presence of a discharge $\epsilon' \neq \epsilon_0$ and ϵ'' and V_L are no longer zero and hence jB_L and G_L are also not zero. As indicated by the equations in Fig. 4, these equivalent circuit elements are nonlinear functions of many experimental variables. These include discharge gas mix and type, pressure and flow rate, discharge geometry, absorbed microwave power (i.e., $|E|^2$) and discharge properties such as electron density and collision frequency. The nonlinear behavior of the discharge (and hence the behavior of the equivalent circuit elements) is exhibited as hysteresis in experimental variables such as input power, tuning, and operating pressure.[7-10,22,23]

The discharge admittance shifts the resonance, unmatching the plasma-loaded cavity from the feed transmission line. If the cavity length and coupling probe remain fixed, further increases in incident power result in only a slight increase in absorbed power and a small change in discharge admittance, since the cavity is further detuned from resonance. Thus the presence of the discharge allows only a small portion of additional incident power into the cavity, causing a large increase in reflected power. This limited variation in discharge properties is a fundamental problem associated with sustaining microwave discharges in fixed-size and fixed-coupling cavities.[22] Discharges in these cavities can be maintained over only a very narrow range of discharge loads (discharge densities, volumes, pressures, flow rates, etc.), and thus these cavity applicators often operate with large reflected powers.

The variable "internal cavity" matching employed in this applicator provides the variable impedance transformation that allows the discharge to be matched over a wide range of discharge loads. The tuning, together with variation of the incident microwave power, "pulls" the discharge properties along a discharge "loss line" similar to that described elsewhere for cylindrical discharges.[7-9,22,23] For a given incident power, gas type, gas flow rate, and discharge pressure, i.e., for a given operating condition, the length and probe tuning are varied iteratively until reflected power is reduced to zero. Typical tuning distances are of the order of several millimeters, and thus the tuning process can be quickly performed either manually or with small motors and can also be utilized as a simple discharge power control technique.

The matching is accomplished without altering either the plasma shape and position or the mode electromagnetic field patterns and without losing microwave power in external (conventional) tuning stubs. Increases in input power increase the electric and magnetic field strengths. However, the geometry of field patterns as shown in Fig. 3, i.e., the electromagnetic focus, remains approximately constant throughout the tuning process, keeping the location of the plasma in the center of the cavity, away from external walls. Thus the cavity system can be tuned to a match as the experimental conditions, such as flow rate, pressure, and discharge configuration, change.

Experimental Apparatus

The experimental measurements were performed with a continuous-wave (CW) variable-power (0–2500 W) microwave system similar to that described elsewhere.[8,9] It consists of 1) a 2.45-GHz, CW, variable-power source, 2) a circulator and matched dummy load, 3) waveguide directional couplers, attenuators, and power meters that measure incident power P_i and reflected power P_r, 4) a coaxial coupling system, and 5) the microwave applicator, i.e, the cylindrical

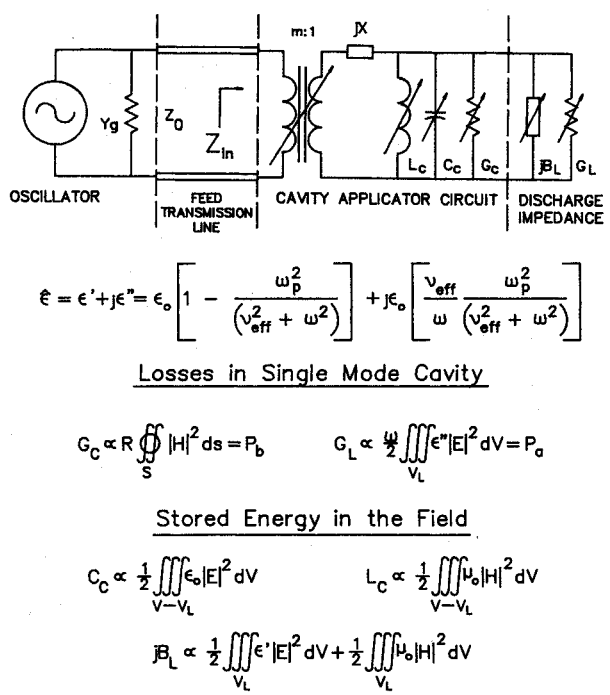

Fig. 4 Equivalent circuit of the single-mode cavity applicator. The intergrals describe the relationship between the equivalent lumped circuit elements and the electric and magnetic fields in a single-mode cavity applicator. Here $\hat{\epsilon}$ is the equivalent discharge dielectric constant.

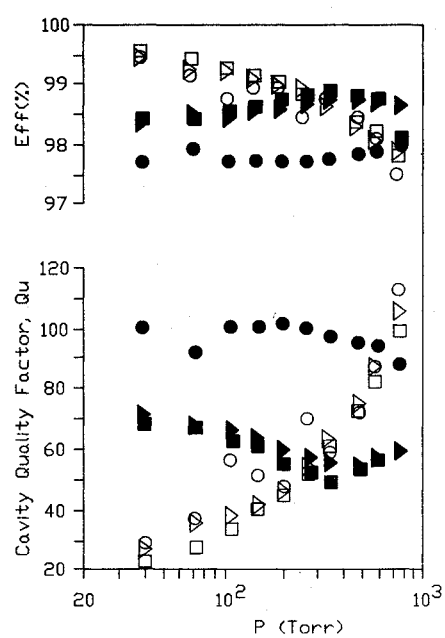

Fig. 5 Microwave coupling efficiency and cavity Q vs discharge pressure for nitrogen and helium gases in different-sized quartz discharge chambers. Open markings and solid markings represent data for nitrogen and helium gas, respectively. Size of quartz discharge chamber: ○, 12 mm; ◁, 25 mm; □, 37 mm. The input power P_t varied from 300 W at low pressure to 490 W at high pressure.

cavity. The microwave power coupled into the applicator is then $P_t = P_i - P_r$.

Experiments were performed using nitrogen and helium gas as propellants, with flow rates of 8×10^{-6} to 150×10^{-6} kg/s. Either the TM_{012} or TM_{011} cavity mode was excited, and all measurements were performed with the cavity applicator in a vertical position. The propellant flowed down the center of the tube and out the nozzle, which was placed at the bottom of the cavity applicator. At the exit of the nozzle a heat exchanger was used to cool exhausted propellant, and a vacuum pump was used to exhaust the propellant and maintain the downstream side of the nozzle at a low pressure (<1 Torr). Hence the nozzle operated in a choked condition. A constant-flow controller was used to measure and maintain flow at a constant flow rate, and an electronic manometer and a Heise gage were used to measure discharge pressure. Forced air cooling of the outer walls of the quartz discharge chamber prevented the quartz from melting, although this cooling reduced the measured energy efficiencies. The nozzle was located at the fixed short (3) of the cavity for all measurements, and brass collars (14) were placed tightly around it to increase the cavity Q and reduce microwave leakage.

No flow experiments were required when measuring discharge coupling efficiency. These experiments were set up as described previously, except that, in addition to the valves associated with the flow controller, a shutoff valve was located downstream from the nozzle so that the tube could first be evacuated to vacuum. Then test gas was allowed to flow into the tube with this valve still open so that any remaining impurities were flushed out. The valve was then closed and gas added to bring it up to the desired test pressure. Since the nozzle was not needed for these no-flow experiments, a straight quartz tube replaced the quartz nozzle.

Measurement of the radial electric field strength $|E_r|$ adjacent to the cavity walls was accomplished by inserting small microcoax electrical probes (13) into the diagnostic holes (12) in the rectangular brass piece (11) shown in Fig. 2. When inserted into one of these equally spaced holes, the probe coupled out a very small fraction of the power proportional to $|E_r|^2$ which was measured with a power meter.

Basic Equations

The evaluation of the thruster performance involved the experimental determination of two figures of merit: 1) the overall energy efficiency η and 2) the specific impulse I_{sp}. This evaluation also involved the experimental measurement of the microwave coupling efficiency. A discussion of these quantities has been given in detail elsewhere,[2,23] and thus they will only be briefly outlined below.

Thruster Performance Figures of Merit

The specific impulse is defined as the ratio of thrust to the propellant mass flow rate expressed in units of seconds. Thus

$$I_{sp} = F/\dot{m}g \tag{1}$$

The overall energy efficiency is defined as the ratio of the output thrust power to the total input power or, more specifically, as the time rate of change of the propellant kinetic energy divided by the sum of the input microwave power and the time rate of change of kinetic energy flow of the initially cold propellant.

$$\eta = \frac{\frac{1}{2}\dot{m}_H v_H^2}{P_a + \frac{1}{2}\dot{m}_c v_c^2} \tag{2}$$

From momentum considerations, the thrust force is given by $F = \dot{m}v$, assuming all mass particles have a uniform velocity parallel to the thrust vector but in the opposite direction,

$$\eta = \frac{(F_H^2/2\dot{m}_H)}{P_a + (F_c^2/2\dot{m}_c)} \tag{3}$$

Note that when the input absorbed power is zero, output conditions correspond to the cold flow input, yielding an efficiency of 100%. In the experimental results presented here the mass flow rate was held constant during the cold and hot measurements; i.e., $\dot{m} = \dot{m}_H = \dot{m}_C$. Thus from Eq. (2) the energy efficiency can be expressed as

$$\eta = \frac{I_{spH}^2}{(2P_a/g^2\dot{m}) + (I_{spc}^2)} = \frac{(I_{spH}^2/I_{spc})}{(2P_a)/(g^2\dot{m}I_{spc}^2) + 1} \tag{4}$$

Also, for a constant hot and cold propellant flow rate the power to thrust ratio can be written as

$$(P/F) = (g/2)[(I_{spH}/\eta) - (I_{spc}^2/I_{spH})] \tag{5}$$

The cold gas specific impulse, assuming full isentropic expansion to vacuum conditions, can be written as[24]

$$I_{spc} = 24.6\sqrt{(T_0/M)}\ \ s \tag{6}$$

for diatomic gases with a specific heat ratio of 1.4 and

$$I_{spc} = 20.9\sqrt{(T_0/M)}\ \ s \tag{7}$$

for monatomic gases with a specific heat ratio of 1.3. In Eq. (6) and (7), T_0 equals the gas temperature prior to expansion and M equals the molecular weight of the gas. With Eqs. (6) and (7), calculated values of the cold specific impulse for nitrogen vary from 79.2 to 81.2 s, and for helium they vary from 177.9 to 182.5 s as the temperature varies from 290 to 305 K. Using nozzles that were not fully optimized, measurements of thrust with a thrust stand were performed on room-temperature gases at constant flow rates. The specific impulse calculated from these measurements yielded values up to 90% of the theoretical values given by Eqs. (6) and (7).

In the experiments described here, the cavity applicator, i.e., the thruster, was connected to rigid microwave cables and thrust could not be measured directly. Thus the specific impulse was calculated from hot and cold measured pressures at a given propellant flow rate. It has been shown that the ratio of measured thrusts between hot and cold conditions for a given propellant flow rate bears a 1:1 relationship with the hot to cold pressure ratio.[2] This relationship is also evident in the equation for thrust, given by

$$F = C_F p A^* \tag{8}$$

The thrust coefficient C_F is a function of the nozzle expansion ratio, the gas specific heat ratio, and the ambient-to-nozzle-exit pressure difference. For a fully expanded nozzle exhausting into vacuum, the thrust coefficient is essentially a function of the specific heat ratio. Experimental observations showed that the measured thrust and the nozzle inlet pressure tend to a maximum concomitantly when the discharge plasma is near the nozzle throat but not through it.

Therefore all experiments were conducted at high pressure (>170 Torr) where the discharges were located upstream from the nozzle and a dark recombination, de-excitation, and gas thermalization space existed between the nozzle and the active discharge. This condition implies that most, if not all, of the dissociated, ionized, and excited species relaxed to approach an equilibrium gas before the propellant passed through the nozzle. At the high pressures and with the gases used here, these are good assumptions. Thus the thrust coefficient differs little from that of the cold molecular gas condition, and as a result the thrust ratio, and hence the specific

impulse ratio, is proportional to the hot-to-cold pressure ratio.

Since specific impulse is proportional to thrust, the energy efficiciency is given by

$$\eta = \frac{(p_H/p_c)^2}{(2/\dot{m}g^2)(P_a)/(I_{spc})^2 + 1} \tag{9}$$

where p_H and p_c equal the hot and the cold pressure of the microwave discharge chamber, respectively. The energy efficiency for the constant-mass flow experiments reported in the following was determined by measurement of the hot and cold pressures, the input microwave power, and the cold specific impulse [i.e., Eqs. (6) and (7)].

Cavity Applicator Equations

The difference between the incident power P_i and the reflected power P_r measures the total power P_t delivered to the applicator. Power delivered into the applicator then divides itself between the power P_b delivered to the conducting cavity walls and the power P_a delivered to the discharge; i.e., $P_t = P_b + P_a$. As shown in Fig. 4, these two quantities can be related to the cavity fields, discharge variables such as the plasma frequency ω_p and the effective collision frequency ν_{eff}, and the intrinsic resistance of the cavity walls. The exact division of the power between the walls and the discharge depends on the relative lossyness of the discharge vs the lossyness of the cavity walls.

It is useful to define another system "figure of merit" called coupling efficiency, which is concerned with the efficiency of coupling microwave power into the discharge. The overall coupling efficiency can be defined as

$$(\text{Eff})_1 = 100 \times (P_a/P_i) \tag{10}$$

where $P_i = P_r + P_t = P_r + P_a + P_b$. If one views the applicator as an impedance transformer and a focusing device, the ideal applicator will deliver all the incident power into the discharge with zero reflected power and applicator wall loss power; i.e., the overall coupling efficiency will then be 100%. In most experiments the reflected power can be reduced to a very small value by tuning adjustments; i.e., $P_r \ll P_i$. Then the overall coupling efficiency is equal to just the applicator coupling efficiency $(\text{Eff})_2$, i.e.,

$$(\text{Eff})_2 = 100 \times (P_p/P_t) = 100 \times (P_a)/(P_a + P_b) \tag{11}$$

Despite the simplicity of this equation, the coupling efficiency is a difficult quantity to determine experimentally, since the wall losses are difficult to measure. However, as discussed below, the single-mode excitation of the applicator allows the approximate measurement[23] of P_b.

Experimental Results

Measurement of Microwave Coupling Efficiency

The coupling efficiency and cavity Q were measured with nonflowing discharges excited in the TM_{012} mode. The measurement technique has been described in detail earlier[23] and thus is only summarized briefly below. An important assumption of the measurement technique is that the presence of the discharge does not significantly alter the spatial distribution of the cavity wall currents from those of the empty cavity TM_{012} mode. Evidence supporting this assumption is that only very small experimental changes in resonant length are required to match the plasma from no discharge to discharge operation; i.e., the discharge in the cavity is a small-length perturbation from empty cavity resonance. Experimental measurements of the axial distribution of $|E_r|$ at the cavity walls with microcoax probes showed the presence of a spatially similar TM_{012} standing wave with or without the discharge. Finally, the exact numerical solutions for the cavity field distributions with the lossy plasma present only differ from the empty cavity distributions near the discharge in the center of the cavity[23]; i.e., the wall current distributions for the TM_{012} mode change very little with the presence of the discharge. Under these conditions, the ratio of the radial electric field measured at a fixed position on the cavity wall to the total power absorbed by the walls is a constant with and without a discharge; i.e.,

$$P_b/|E_r|^2 = \text{const} \tag{12}$$

By measuring the power absorbed P_{t0}, cavity quality factor, Q_{u0}, and the associated radial electric field E_{r0} for the critically coupled, empty cavity excited by a low-power test signal, the power P_b, absorbed by the walls, and Q_u for a cavity loaded with a discharge can be determined from the following equations[23]:

$$P_b = (|E_r|^2/|E_{r0}|^2)P_{t0} \tag{13}$$

$$Q_u = (Q_{u0}P_{t0}/|E_{r0}|^2)(|E_r|^2/P_t) \tag{14}$$

where $|E_r|$ and P_t are, respectively, the radial electric field and cavity absorbed power with the discharge present. Since both equations require the ratios of the electric fields, only relative magnitudes of electric fields are necessary.

Using a single microcoax probe located at a standing wave E_r maximum, the coupling efficiency, i.e., Eq. (11), and the corresponding Q_u were determined for nonflowing He and N_2 discharges excited with the TM_{012} mode. The results, shown in Fig. 5, are displayed for a pressure range of 40–800 Torr and for several discharge tube diameters. These results clearly indicate that the coupling efficiency is in excess of 97% for all discharge conditions. The cavity Q with the discharge present is relatively low, varying from 20 to 110. These measurements were taken for the no-flow case, since electric field measurements require a steady cavity field, an impossible condition for flowing discharges, where the discharge and hence the cavity fields are no longer completely stationary. The coupling efficiencies and the loaded Q differ little for the flowing gas discharges, since the major difference is that the flowing gases carry away some of the discharge energy that would otherwise be conducted to the discharge chamber walls. Thus the transfer of microwave energy to the discharge is very efficient over the experimental pressure range of interest for the electrothermal thruster, and $P_t \simeq P_a$ for the thruster measurements discussed in what follows.

Electrothermal Thruster Measurements

The desirable experimental configuration for thrust measurement was to ignite an axially vertical discharge separated from the discharge chamber walls. The discharge was maintained along the axis of the discharge chamber as shown in Figs. 2 and 3, where an input gas flows around and through the discharge. Gas heating occurs 1) by radial heat transfer from the discharge center to the cooler external gas layer and 2) by direct heating of gases that pass through the hot discharge. Downstream from the plasma the hot and cold gases mix to produce a relatively high-temperature gas at the nozzle. For all the experiments reported here, it is believed that gas flows were laminar with a calculated friction drop of, at most, 39 Torr. Thus the pressure of the discharge zone was essentially equal to the measured upstream pressure. In a few experiments a quartz centerbody [(10) in Fig. 2] was used as a flow stabilizer. It served the dual purpose of forcing boundary layer flow along the inner surface of the tube and of providing a "wake" or recirculating zone similar to a combustion stream flameholder. Without the centerbody, a critical flow velocity was reached when the plasma discharge zone was swept downstream from the intense microwave

Table 1 Experimental conditions for Figs. 6-8

Point	Gas	Flow rate, kg/s × 10^{-6}	Discharge pressure, Torr	Cavity mode	Nozzle size, mm	Stabilization of centerbody
● [a]	N_2	63.0	503-525	TM_{012}	1.17	Yes
■ [a]	N_2	104	710-819	TM_{012}	1.17	Yes
▲ [a]	N_2	146	953-1021	TM_{012}	1.17	Yes
◂	N_2	36.5	380-440	TM_{011}	1.17	No
◆	N_2	146	882-1000	TM_{011}	1.17	Yes
○	He	26.7	280-328	TM_{012}	1.17	No
□	He	8.9	170-196	TM_{011}	1.17	No
△	He	14.8	260-320	TM_{011}	1.17	No
◇	He	20.8	330-430	TM_{011}	1.17	No
◁	He	26.7	402-546	TM_{011}	1.17	No
⊙	He	8.9	567	TM_{011}	0.51	No
▽	He	10.4	625	TM_{011}	0.51	No
⊙	He	11.9	810	TM_{011}	0.51	No

[a]Reproduced from Ref. 2.

field region and extinguished. During well-tuned operation, the upstream edge of the plasma zone barely contacted the tip of the flow stabilizer. Formation of the stable incoming flowfield pattern was essentially completed in the unheated gas region upstream of the plasma zone and thus was independent of the reaction process in the plasma zone.

Experimental runs were performed by first establishing a desired propellant flow rate and holding this flow rate constant through the entire run. The cold discharge chamber pressure p_c was measured. The discharge was then ignited, the input microwave power adjusted, and the applicator input power P_t and the steady-state discharge pressure p_H measured. After each experimental run, the discharge chamber was allowed to cool back to "cold" conditions as a check against significant nozzle erosion. As discussed previously the microwave coupling efficiency is very high, and thus the energy efficiency, the thrust-to-power ratio, and the specific impulse can be calculated from Eqs. (5-7) and (9). Figures 6-8 summarize typical experimental results, and Table 1 details the different experimental configurations and operating points.

All data presented in Fig. 6-8 were taken with quartz discharge chambers of inner diameter 28 mm. Experimental runs were taken for preset constant-input gas flow conditions, and several operating points were taken as the input power was continuously increased from a low initial value. Data points from separate constant-flow experimental runs are joined together as curved lines in Figs. 6-8. The input power was increased until heating threatened to destroy the quartz nozzle. Thus the maximum input power of each experimental run was limited by nozzle heating. Data points from earlier reported experiments[2] in N_2 gas excited in the TM_{012} mode are displayed in Figs. 6-8 for comparison.

The discharge behavior in the TM_{012} mode was similar to that observed in previous experiments[2]; however, when exciting the TM_{011} mode, the discharge was next to but not quite touching the nozzle, as shown in Fig. 3. For both modes the discharge lengths and diameters (hence size) increased as input power increased, and decreased or constricted slightly as pressure or flow rate increased. As can be seen from the data, helium gas excited with the TM_{011} mode has higher energy efficiencies than in the TM_{012} mode. Energy efficiencies also increase with higher flow rates and higher operating pressures and smaller nozzle sizes.

Since the energy deposited in the gas is known, it is of interest to compute an equilibrium, fully mixed temperture for these experiments and compare these results with the I_{sp} and energy efficiency given in Figs. 6-8. An approximate calculation can be made by using a steady-state constant-mass flow rate and a one-dimensional flow model for the input and exit

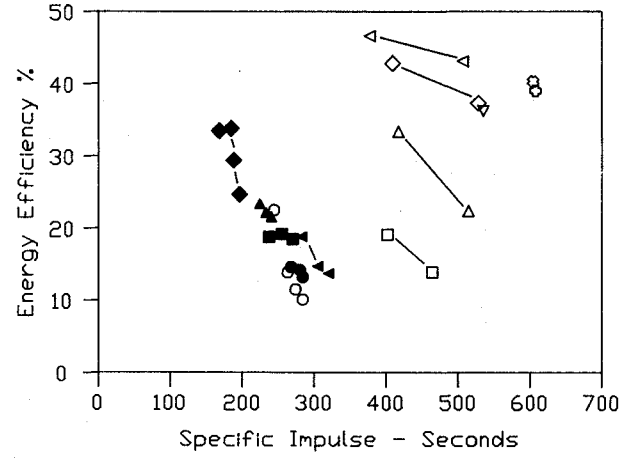

Fig. 6 Energy efficiency vs specific impulse for the different experimental conditions listed in Table 1.

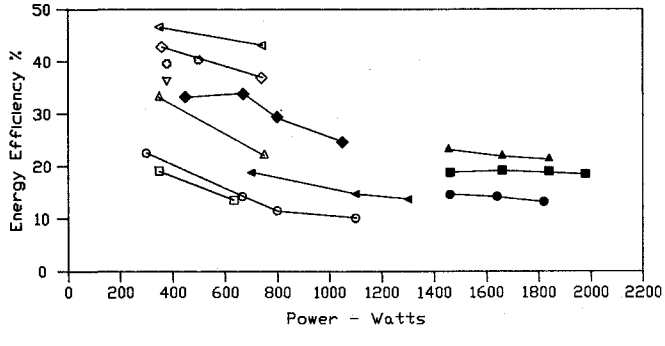

Fig. 7 Energy efficiency vs power absorbed in the cavity applicator for the different conditions described in Table 1.

planes of the discharge zone. Under these assumptions, it can be shown that

$$C_p(T_{02}-T_{01})=P_a/\dot{m} \tag{15}$$

If the specific heat as a function of temperature is known, the left-hand side of Eq. (15) can be obtained by integration between the inlet temperature and the desired outlet temperature T_{02}. This temperature can also be obtained from thermodynamic tables. The thermophysical properties of nitrogen at elevated temperatures were available to the

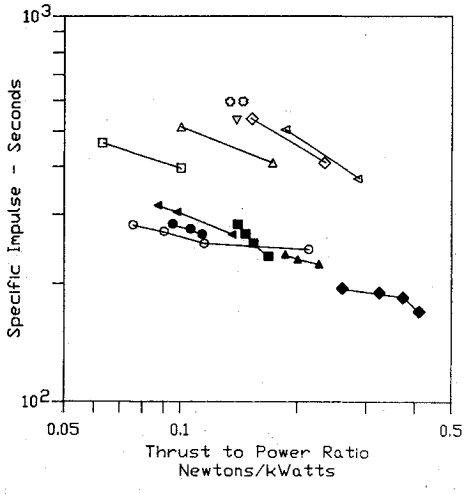

Fig. 8 Specific impulse vs thrust-to-power ratio for the different conditions listed in Table 1.

authors up to only about 3000 K. A separate table gave the specific heat at a constant pressure and specific heat ratio of 1332.2 J/kg K and 1.287, respectively at 3550 K. A typical set of nitrogen test data at a mass flow rate of 146×10^{-6} kg/s and a power level of 450–1050 W corresponded to a specific energy input of 3.08×10^6 to 7.2×10^6 J/kg. The equilibrium gas temperatures for the corresponding enthalpy change above 300 K were 2827–5705 K, and specific heat ratios of 1.31–1.287 were assumed. The theoretical specific impulses at these temperatures are 271.8–397.7 s, compared with 170–200 s obtained experimentally. Since efficiency varies directly as I_{sp}^2, and if the theoretical (calculated) I_{sp} is associated with an efficiency of 1.0, then the measured efficiency is equal to the square of the ratio of the measured to the theoretical I_{sp}. For the conditions described previously, the efficiencies are 0.39–0.25 and compare favorably with the efficiencies shown in Figs. 6–8.

A similar comparison for a typical run with helium at a flow rate of 26.7×10^{-6} kg/s yielded theoretical specific impulse values of 532–789 s. The specific impulse values obtained from pressure measurements were 375–510 s. The efficiencies calculated as the ratio of the specific impulse squared were 0.496 and 0.417, which also agreed favorably with the values in Fig. 8.

Summary and Conclusions

These experimental results further support the microwave electrothermal thruster concept. Measurements on static N_2 and He discharges clearly show that the microwave coupling efficiency to these gases is in excess of 95% over a pressure range of 40 Torr to 1.5 atm; i.e., the transfer of microwave energy to these discharges is a very efficient process. The experimental runs in the gas were carried out over nozzle sizes of 0.5–1.3 mm and a tube inside diameter of 28 mm and were limited to discharge pressures of <1100 Torr. Excessive heating and erosion of the quartz nozzles limited input power levels to <2000 W at the high flow rates of 60×10^{-6} to 150×10^{-6} kg/s and even became a problem with 400 to 700 W at the lower flow rates of 50×10^{-6} kg/s. Thus the material erosion of the quartz nozzle limited the calculated specific impulse to <550 s. The energy efficiencies in He gas, determined by measuring hot and cold discharge pressures and achieved by exciting the cavity in the TM_{011} mode, were similar to those in N_2 gas[1,2] and were comparable to other electrothermal thrusters.[3-5]

These experiments represent data from a first-generation prototype. Forced air cooling was employed to cool the quartz walls of the nozzle and discharge chamber during all measurements, resulting in reduced energy efficiencies. It is clear from experimental data together with earlier results[1,2] that the thruster performance is dependent on the discharge chamber size, the nozzle size, the discharge position, pressure, propellant flow, etc. The prototype thruster used in these experiments does not represent an optimized design, since no attempt was made to minimize loss mechanism. A significant improvement in performance may result from optimization of the flow configuration for better energy transfer and lower thermal losses. Higher-temperature nozzle materials should improve the specific impulse, and a redesign of the cavity can greatly reduce the applicator size and weight.

This microwave electrothermal concept has several potential advantages over the more conventional methods of electrothermal propulsion, such as the resistojet and arcjet. One obvious advantage is the absence of electrodes inside the discharge zone, eliminating the power loss and lifetime and materials problems produced by the electrodes. A further advantage is the ability to focus power at high pressure into a controllable microwave arc separated from enclosure walls. A discharge zone with a hot core is formed in the center of the discharge chamber walls. Since the hot core readily absorbs microwave energy, very high electric energy fluxes can be coupled directly to the gaseous propellant without melting and eroding discharge chamber walls and thereby minimizing material and lifetime problems. Helium gas was used in these experiments for safety and convenience, but other gases, such as H_2, mixtures of H_2 and N_2, oxidizing gases, and even water vapor, can be used as a propellant without electrode erosion problems.

Important but more subtle advantages are associated with the design freedoms allowed with this microwave concept. There are no electrodes in the discharge zone, and the electromagnetic coupling of the electrical energy into the discharge can be controlled externally to the discharge chamber with cavity mode excitation, tuning, and input power control. Thus the efficient coupling to the high-temperature discharges and the minimization of energy losses for the discharge are no longer strongly interdependent. As a result, the discharge chamber geometry, i.e., its size and shape, the position of the discharge with respect to the nozzle, the propellant flow rate, and the flow configuration (vortex, etc.) can all be varied to yield an optimized thruster performance with little effect on the efficiency of the electromagnetic coupling. The discharge chamber can be constructed for minimum energy losses and maximum thrust, while the surrounding microwave applicator is designed for high-efficiency microwave coupling.

Acknowledgment

The authors would like to acknowledge the support of this research by NASA Lewis Research Center, Contract NAG 3-305.

References

[1]Whitehair, S., Asmussen, J., and Nakanishi, S., "Demonstration of a New Electrothermal Thruster Concept," *Applied Physics Letters,* Vol. 44, May 1984, pp. 1014–1016.

[2]Asmussen, J., Whitehair, S., and Nakanishi, S., "Experiments with a Microwave Electrothermal Thruster Concept," AIAA/JSASS/DGLR 17th International Electric Propulsion Conference IEPC 84-74, Tokyo, Japan, May 1984.

[3]Zafran, S. and Jackson, B., "Electrothermal Thruster Diagnostics," Vols. I and II, TRW Space Technology Group, NASA CR 168174, May 1983.

[4]Page, R. R. and Stoner, W. A., "The Design and Technology Development of a 150 MLB Resistojet for H_2 or NH_3," AIAA Paper 82-1949, 1982.

[5]Wallner, L. E. and Czika, J., "Arc-Jet Thruster for Space Propulsion," NASA TND-2868, June 1965.

[6]Frasch, L. and Asmussen, J., "Electrothermal Propulsion of Spacecraft with Time-Varying Electromagnetic Energy," AIAA Paper 85-2050, 1985.

[7]Fredericks, R. M. and Asmussen, J., "High-Density Resonantly Sustained Plasma in a Variable-Length Cylindrical Cavity," *Applied Physics Letters,* Vol. 19, 1971, pp. 508-510.

[8]Asmussen, J., Mallavarpu, R., Hamann, J. R., and Park, H. C., "The Design of a Microwave Plasma Cavity," *Proceedings of the IEEE,* Vol. 62, Jan. 1974, pp. 109-117.

[9]Mallavarpu, R., Hawley, M. C., and Asmussen, J., "Behavior of a Microwave Cavity Discharge over a Wide Range of Pressures and Flow Rates," *IEEE Transactions on Plasma Science,* Vol. PS-6, Dec. 1978, pp. 341-354.

[10]Kapitza, P. L., "Free Plasma Filament in a High Frequency Field at High Pressure," *Soviet Physics JETP,* Vol. 30, June 1970, pp. 973-1007.

[11]Baltin, L. M., Batenin, V. M., Devyatkin, I. I., Lebedeva, V. P., and Tsemko, N. I., "Stationary Microwave Discharge in Nitrogen at Atmospheric Pressure," *High Temperature,* Vol. 9, Nov.-Dec. 1971, pp. 1019-1025.

[12]Arata, Y., Miyake, S., Kobayashi, A., and Takeuchi, S., "Research of a Stationary High Power Microwave Plasma at Atmospheric Pressure," *Journal of the Physical Society of Japan,* Vol. 40, May 1976, pp. 1456-1461.

[13]Batenin, V. M., Zrodnikov, V. S., Roddatis, V. K., and Chinnov, V. F., "Experimental Investigation of a Microwave Discharge in Helium," *Soviet Journal of Plasma Physics,* Vol. 2, Sept.-Oct. 1976, pp. 463-466.

[14]Franklin, R. N., *Plasma Phenomena in Gas Discharges,* Clarendon, Oxford, 1976, pp. 94-103.

[15]Pfender, E., "Electric Arcs and Arc Gas Heaters," Vol. I, *Gaseous Electronics,* M. N. Hirsch and H. J. Oskam, eds., Academic, New York, 1978, pp. 291-398.

[16]Elenbass, W., *Light Sources,* Crane, Russak, New York, 1972.

[17]Cherrington, B. E., *Gaseous Electronics and Gas Lasers,* Pergamon, Oxford, 1979, pp. 156-159.

[18]Asmussen, J. and Root, J., "Characteristics of a Microwave Plasma Disk Ion Source," *Applied Physics Letters,* Vol. 44, Feb. 1984, pp. 396-398.

[19]Asmussen, J. and Root, J., "Ion Generating Apparatus and Method for the Use Thereof," U.S. Patent No. 4 507 588, March 26, 1985.

[20]Root, J. and Asmussen, J., "Experimental Performance of a Microwave Cavity Plasma Disk Ion Source," *Review of Scientific Instruments,* Vol. 56, Aug. 1985, pp. 1511-1519.

[21]Ramo, S., Whinnery, J. R., and Van Duze, T., *Fields and Waves in Communications Electronics,* 1st ed., Wiley, New York, 1972, p. 566.

[22]Halverson, S. L. and Hatch, A. J., "Frequency-Shifting Method of Exciting a Plasma in a Resonant Cavity," *Applied Physics Letters,* Vol. 14, Jan. 1969, p. 79.

[23]Rogers, J., "Properties of Steady State, High Pressure Argon Microwave Discharges," Ph.D. Thesis, Michigan State University, 1982.

[24]Hawkins, C. E. and Nakanishi, S., "Free Radical Propulsion Concept," NASA TM-81770; also AIAA Paper 81-0676, 1981.

[25]Harrington, R. F., *Time-Harmonic Electromagnetic Fields,* McGraw-Hill, New York, 1961.